Machine Learning Approaches for Analysis of Total Ionizing Dose in Microelectronics

B. Dean, *Student Member, IEEE,* T. Peyton, *Student Member, IEEE,* J. L. Carpenter, *Student Member, IEEE,* D. Sam, *Student Member, IEEE,* A. Peterson, *Student Member, IEEE,* J. Kim, *Student Member, IEEE,* S. P. Lawrence, *Student Member, IEEE,* M. Fadul, *Student Member, IEEE,* D. R. Reising, *Senior Member, IEEE* and T. D. Loveless, *Senior Member, IEEE*

***Abstract*—Supervised deep learning is a subset of machine learning (ML) that allows for the development of phenomenological models based on measured observations through layered artificial neurons. A convolutional neural network (CNN) is one model typically used in image recognition that allows for classifying behavior in discrete sets or enabling regression analysis. This work demonstrates a one-dimensional CNN to analyze irradiated commercial off-the-shelf (COTS) electronics. COTS microcontroller units (MCU) were irradiated with 10 keV X-rays, and CNN models were trained on the resulting internally generated noise signatures from the clock module. As a result, the MCUs are accurately classified as either fresh or dosed, and the total ionizing dose (TID) is predictable through a regression model. This approach allows for part dosimetry and in situ device health monitoring without additional components.**

***Index Terms*—Convolutional Neural Network, Machine Learning, Radiation Effects, Total Ionizing Dose, Regression, Classification, Complex Digital Device.**

I. Introduction

THE continuous increase in complexity of microelectronics allows for more efficient use of silicon area and performance increases. In recent years, scaling limitations have been overcome through multi-component systems-on-chip (SoC), multi-die systems-in-package (SiP), heterogeneous integration (HI) schemes, and three-dimensional integrated circuits (3DIC) solutions. Moreover, these complex ICs are becoming more interconnected. For example, a rising number of spacecraft are being launched due to the increased commercialization of space that use system-level mitigation methodologies to ensure network reliability and radiation tolerance. Analysis and isolation of radiation vulnerabilities in complex systems (network level or IC level) are complicated due to the many inaccessible internal components. Radiation-hardening-by-design (RHBD) is often not feasible for these complex commercial-grade components. Automated system health telemetry that includes reliability and radiation response metrics can provide helpful guidance for assessing risk and ensuring spacecraft survivability; however, radiation telemetry generally requires additional components for conducting dosimetry and only documents radiation environments, not component responses. Real-time knowledge of system radiation response health can aid in diagnosing and alleviating possible issues.

This paper describes the use of machine learning (ML) to identify total ionizing dose (TID) exposure in a mixed-signal commercial-off-the-shelf (COTS) processor without the need for external components and using only signals emitted from the processor. Experiments were conducted on several microcontroller units (MCU) manufactured by Texas Instruments, irradiating the devices while biased in different low-power modes (LPM) or idle sleep states. Clock output signals were measured following irradiation in three different LPMs to investigate how internal circuit biasing affects TID impact. A convolutional neural network (CNN), trained purely on the internally generated noise within the clock signals, was used to develop models for binary classification of dosed versus non-dosed devices and regression to predict the TID value.

II. Background

A. Total Ionizing Dose Effects in Systems-on-Chip

TID effects result from charge trapping in oxide insulators and oxide-semiconductor interfaces. Due to their lower mobility, holes are trapped more often than electrons and can cause undesired responses in ICs. For example, transistor shifts in threshold voltages, increases in leakage current, and degradation in transconductance can result in increased power, degradation in clock frequencies, decreased performance, and long-term damage to semiconductor oxide layers, with inevitable failure [1]. Fig. 1 displays an example of the increase in average current consumption of one of the several clock modules within a TI MSP430FR6989 MCU following irradiation. In this case, the MODOSC clock module was enabled post-irradiation, and the MCU irradiated in low-power mode 0 (LPM 0), see Table I, which disabled the CPU and the primary clock channel (MCLK) while keeping the clock sources active. Negligible changes in DC current consumption are visible until 30 krad(SiO_2) when the current increases until device failure at approximately 60 krad(SiO_2).

B. State of the Art SoC Testing and Dosimetry

For transistor-level TID testing, experimentalists must determine the worst-case bias condition for irradiation, which is

This work was supported in part by the DoD through the SCALE Microelectronics Workforce Development program and the DoD/NSF REU program through award #1757777.

At the time of this work B. Dean was with the University of Tennessee at Chattanooga and is now at Vanderbilt University. T. Peyton, J. L. Carpenter, D. Sam, A. Peterson, J. Kim, S. P. Lawrence, M. Fadul, D. Reising, and T. D. Loveless are with the University of Tennessee at Chattanooga, 615 McCallie Ave., Dept. 2342, Chattanooga, TN, 37403, USA; Phone: 423-425-2353, Fax: 423-425-5229, Email: daniel-loveless@utc.edu

TABLE I: Power Mode Options in the MSP430

Power Mode	Description
Active	CPU is active, and clocks are enabled
LPM 0	The primary clock signal (MCLK) and CPU are disabled
LPM 1	The DCO clock source and DC generator are disabled
LPM 2	The secondary clock (SMCLK) signal is disabled, and DC generator remains active
LPM 3	SMCLK and DC generator are disabled
LPM 4	Low frequency clock (ACLK) signal and all clock sources are disabled
LPM 3.5/4.5	Power management module is disabled

*Each LPM inherits the rules of the lower LPM modes unless otherwise noted (*e.g.* LPM 1 disables the MCLK signal, CPU, and the DCO clock source).

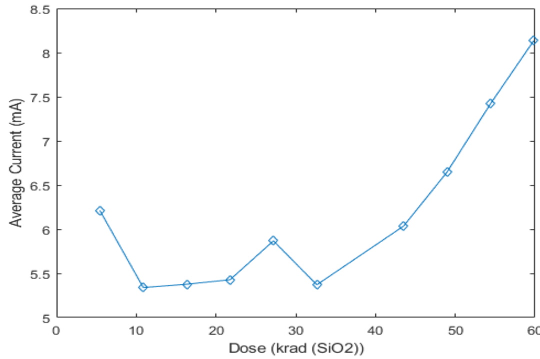

Fig. 1: Example measurement of average current vs. TID for an MSP430FR6989 running the MODOSC sub-circuit post-irradiation. The device was biased in LPM 0 during irradiation.

most often the OFF state bias. However, determining a worst-case response is problematic for SoCs and may involve in situ irradiation. In this work, the MCUs were irradiated under several low-power modes (LPM), described in Table I, which turned off several internal modules and placed the device in various states of “sleep” while being irradiated. The worst-case bias condition depended on the internal component being interrogated during the experiment.

While guidelines for single-event effects (SEE) testing of SoCs have emerged in recent years [2], [3], the current state-of-the-art methods for TID testing on SoC are mainly limited to pass-fail testing due to the inherent complexity and inaccessible terminals. Often, devices are irradiated until communication between the MCU and the host computer fails, denoted as the TID limitation [4]. TID testing of SoCs generally involves irradiating the DUTs, pausing at discrete dose steps, and characterizing the DUT performance [1], [4]–[6]. Characterization may involve many electrical tests or simply the monitoring of power consumption to provide information regarding the overall TID limit of the device. Additional information obtained during TID testing beyond the overall dose limitation may aid in understanding specific component vulnerabilities, allowing designers to program the devices based on specific mission constraints.

Moreover, once a part has been deployed in a system, the TID can be measured using specialized external hardware, such as a dosimeter. Improvement and innovation of dosimetry techniques is a large and continuing area of research. Current techniques include using RADFETs, floating-gate MOSFETS, and highly specialized on-chip circuitry such as a Photocurrent-controlled Oscillatory (PCO) [7]–[9]. Here, utilizing ML, TID is accurately predicted using only the clock signal noise of a microcontroller.

C. Convolutional Neural Networks

Recent works have demonstrated the feasibility of supervised machine learning (ML) strategies for the identification of TID degradation [10] and single-event transients (SET) [11], [12] through the use of k-nearest neighbors (KNN) algorithms. These papers analyze data from irradiated CMOS phase-locked loop circuits; however, the KNN classifiers were limited to only identifying the presence of radiation degradation through a binary classifier or identifying discrete TID levels through multi-bin classifiers. Additionally, KNN models require storing all training data and are difficult to scale. Consequently, it can be computationally expensive to evaluate new data with KNN. This effort uses a supervised deep learning technique that leverages artificial neural networks to develop a model for analyzing TID data through a binary classifier and a regression model for predicting a specific dose level for an exposed part.

CNNs are a subset of ML and are deep learning algorithms commonly used in image recognition applications due to their ability to extract high-level features, although they can also be used for one-dimensional data sets. CNNs can be used to design classification and regression models to make predictions with new measurements. Classification categorizes observations into a finite number of discrete classes, while regression outputs a continuous, non-restricted value.

A CNN works by sliding a kernel (filter) across a layer output and performing matrix multiplication with the kernel and each window to identify low-to-high-level features. This process is similar to the statistical window analysis presented in [11]. A pooling layer is then used to reduce the spatial size of the layer output, which decreases computational cost. These steps can be repeated as many times as needed to extract higher-level features. The resulting features are then flattened and fed into a fully-connected layer, which applies variable weights to the output to increase or decrease the significance of each output. Finally, a loss function is used to

evaluate how well a model performs and to update the output weights to improve accuracy. For example, classification is obtained using a loss function such as CrossEntropy, while regression is obtained using mean-squared error (MSE) as a loss function. In addition, regression and classification models use the rectified linear unit (ReLU) activation function.

III. CNN Architecture

The CNN architecture used in this work for developing classification and regression models is shown in Fig. 2. The CNN consists of three convolutional layers, each followed by a max-pooling layer except the final one. Each convolutional layer uses twelve kernels to extract varying features, creating twelve feature vectors. Following the last convolutional layer, a flattening layer converts the resulting stack of feature vectors into a single one-dimensional (1D) vector. The classification architecture (seen at the top of Fig. 2) uses a Dense layer and the SoftMax activation function to calculate the prediction probabilities for each class. Here, a binary classifier (2 classes) was used to determine if TID is less than 25 krad(SiO_2), denoted as "Fresh," or greater than 25 krad(SiO_2), denoted as "Dosed." The regression architecture (seen at the bottom of Fig. 2) feeds the output of the flattened layer into a Dense layer containing one neuron. Each convolutional layer uses L2 regularization, and dropout was added after flattening to prevent over-fitting. The ML models were built in Visual-Studio Code using the Python programming language.

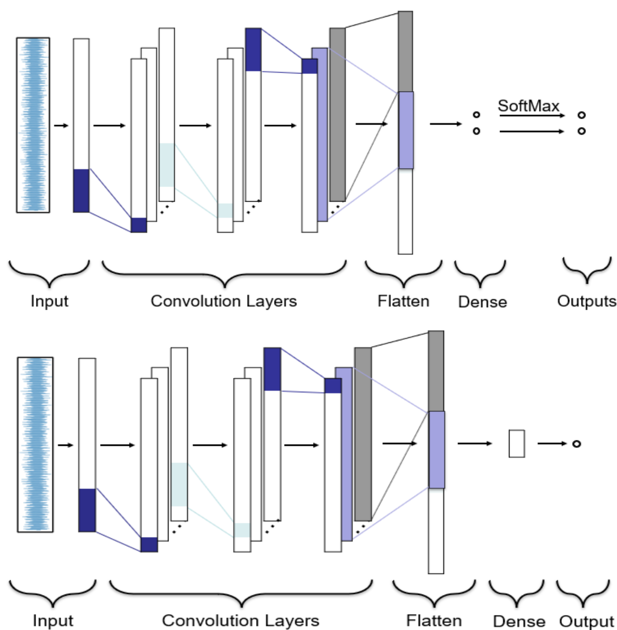

Fig. 2: Convolutional Neural Network (CNN) Architecture of the classification (top) and regression (bottom) models.

IV. Experimental Setup

A. Devices Under Test

The devices under test (DUT) were Texas Instrument's (TIs) MSP430FR6989 (MSP) mixed-signal microcontroller units. Five DUTs were tested in LPMs 0, 2, and 4 to investigate varied susceptibility to radiation effects. Two clock sources were specifically interrogated: the programmable digitally-controlled oscillator (DCO) and the fixed-frequency very-low-frequency oscillator (VLO). TI's EnergyTrace technology also measured real-time current, energy, and power consumption. The MSP was configured using the Code Composer Studio (CCS) IDE in computer language C.

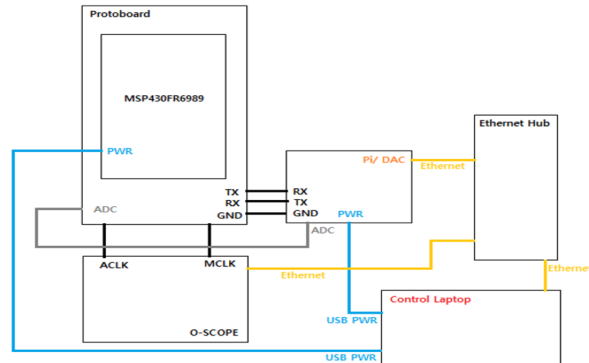

Fig. 3: Block diagram of the measurement setup for the Xray irradiation of the MSP430FR6989.

The five MSP devices were tested at Vanderbilt University using the 10 keV ARACOR X-ray source. All MSPs were biased at 3.3 V during irradiation and measurement. However, several LPMs were used to turn off peripheral circuits within the MSP during irradiation. Three of the DUTs were biased in LPM 4 (lowest power consumption), whereas the other two were biased in LPM 0 (highest power consumption) and LPM 2 (median power consumption). All DUT packages were de-lidded to expose the underlying die. In addition, the DUTs were irradiated at 5.44 krad(SiO_2)/min at dose increments of 2.72 krad (SiO_2) or 5.44 krad (SiO_2). Testing continued until a maximum dose of 60 krad (SiO_2) or when the DUT malfunctioned. At each incremental dose point, the DUT was biased in the active power mode (all peripheral modules biased on), and measurements of the current consumption, clock frequencies, and analog-to-digital (ADC) performance were conducted.

Two clock sources within the MSP's clock system (CS) module were activated using C-code in the MSP's integrated development environment (IDE). The VLO clock source (measured to be approximately 8 kHz for each of the five DUTs) was activated via the auxiliary clock (ACLK) signal path, and the programmable DCO (set to 16 MHz) was activated with the master clock signal path (MCLK). Here, results are limited to the output data associated with the ACLK signal path and the VLO clock source. In addition, a Tektronix DPO7104 oscilloscope (O-Scope) was programmed using Python to record the waveform of each clock.

The MSP was attached to a custom test board that interfaced the DUT with the O-Scope, a digital to analog converter (DAC), and the host computer. The connections to the O-Scope were for measurement of the clock signals. The DAC enabled testing of the on-chip analog-to-digital converter (ADC), and the host computer was used to program the MCU and receive

data. The O-scope was programmed using the Python computer language and Jupyter Notebook, a web-based computing platform, to capture at least 100 periods of the clock signal waveform at each trigger initiated by the host machine; data were saved to a CSV file for post-processing and training of the CNN models.

The DUT was programmed using the C programming language to configure the DUT in the LPMs or activate and run a benchmark program. A benchmark program invoking the VLO clock source on the ACLK line was used in this case. The DAC was managed by a Raspberry Pi (Pi) to measure and analyze the MSP's ADC. In this case, the digital output of the ADC can be converted to an analog signal for processing.

The clock connections were made using coaxial cables and BNC connectors. Finally, the Pi, host computer, and the O-Scope were connected to an ethernet hub to communicate. After the modules were activated and the measurements conducted, the EnergyTrace profiles were saved. Fig. 3 displays a schematic illustrating all connections during testing.

B. CNN Model Training

Several CNN models were developed, including one trained on the raw waveforms; however, the CNN classifier resulted in poor performance when the primary clock frequency was not removed. Trade-offs in accuracy and training time of using different signal characteristics may be of interest in future works. The standardized noise signal was chosen to train the models due to the well-understood relationship between transistor-level noise and radiation. Increases in charge at oxide-silicon interface trap sites following radiation exposure can result in increased capture and emission of carriers with increasing TID, leading to decreased noise figures and increased 1/f noise [13].

The CNN models were trained with data measured on the ACLK signal line, removing the primary frequency component of approximately 8 kHz from the signal before passing the data to the model. The noise signal of ACLK was obtained by standardizing the data set using the z-score according to (1) where X is the observed at time step t, μ is the signal mean, and σ is the signal standard deviation. The absolute value of the clock data was taken before standardization so that the mean could be subtracted from each value regardless of the high or low state of the clock. Fig. 4 illustrates an example measurement of the VLO clock via the ACLK signal line and the resulting noise signal extracted via (1).

$$z = \frac{X - \mu}{\sigma} \tag{1}$$

At each dose increment, $50,000$ clock cycles were measured. Windows of $1,000$ cycles each were randomly sampled from the original signal to increase the number of CNN inputs. The windows were randomly segmented into training, validation, and testing sets to prevent overfitting based on time dependencies; 60% of these data were used to train the CNN models, whereas 20% of these data were used to check the accuracy of the models. The final 20% of the measurements were used to test the ability of the models to evaluate new, unseen data. Three separate models were developed for the

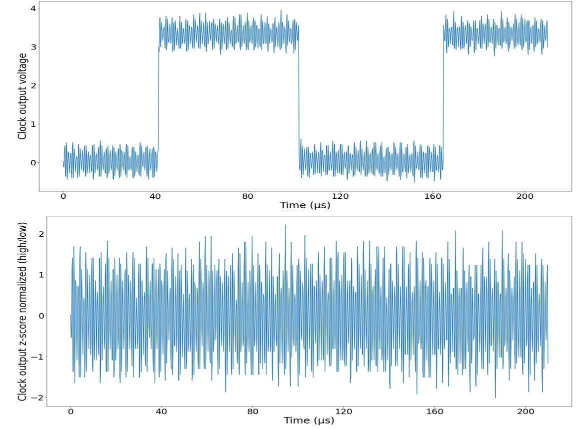

Fig. 4: Example measurement of the VLO clock on the ACLK signal line (top). Also shown is the extracted noise signal (bottom) used to train the CNN models.

DUTs biased in LPM modes 0, 2, and 4 during irradiation. The CNNs were trained with a batch size of $2,048$ time steps and for up to 80 and 40 epochs for the binary classifier and regression models, respectively. Higher accuracy may be obtained through experimentation of batch size and the number of epochs.

V. Results

A. Binary Classification Model

Classification results are presented in confusion matrices, as shown in Table II. The confusion matrices show the number of correct dosed predictions (true positive or TP) and correct fresh (un-irradiated) predictions (true negative or TN). The matrix also displays the number of incorrect dosed predictions (false positive or FP) and incorrect fresh predictions (false negative or FN). Positive predictive value (PPV), given by (1), represents how well the model can predict a device is dosed, and negative predictive value (NPV), given by (2), represents how well the model predicts a new (fresh) device.

$$PPV = \frac{TP}{TP + FP} \tag{2}$$

$$NPV = \frac{TN}{TN + FN} \tag{3}$$

TABLE II: Confusion Matrix Legend for Binary Classifier

Power Mode		Actual Class		
		Dosed	Fresh	
Predicted Class	Dosed	TP	FP	PPV
	Fresh	FN	TN	NPV

The binary classification model assigns data to one of two categories representing a radiation dose of 0-25 krad(SiO_2) (*i.e.,*fresh) or 25-60 krad(SiO_2) (*i.e.,*dosed). The CNN architecture is identical to that used for regression; however, a softmax activation function assigns a probability to the two classes. The CNN model is trained using back-propagation to optimize binary cross entropy loss. The model was trained with

a batch size of 2048 and 80 epochs. The classification needs approximately twice as many epochs as the regression model to converge to a low loss. The increase in training (train) and validation (val) accuracy is shown in Fig. 5 for DUTs biased in LPM 0, 2, and 4. The model trained from data when the MCU was biased in LPM 0, which keeps all clock sources active and disables the MCLK signal line and the CPU, converges to an accuracy of approximately 80% after 40 epochs.

Similarly, the devices irradiated under LPM 2 converge at approximately 40 epochs with higher accuracy. LPMs 0 and 2 maintain the VLO functionality; thus, the DUTs were biased ON during irradiation. However, the model trained from data when the DUT was biased in LPM 4 showed superior performance, the training and validation accuracy converging to approximately 90% accuracy after 30 epochs. This quicker convergence is likely due to the monotonic shifts with TID while the VLO module was biased OFF during irradiation (*i.e.,* less competing effects). The confusion matrices are illustrated in Table III, and the total accuracy of the classifier is shown in Table IV, indicating 100% PPV for dosed devices irradiated under LPM 4, with a total accuracy of approximately 90%.

TABLE III: Classification Results for DUTs Biased in LPMs 0, 2, and 4

LPM 0		Actual Class		
		Dosed	Fresh	
Predicted Class	Dosed	442	104	81.0%
	Fresh	28	290	91.2%
LPM 2		Actual Class		
		Dosed	Fresh	
Predicted Class	Dosed	431	17	96.2%
	Fresh	39	377	90.6%
LPM 4		Actual Class		
		Dosed	Fresh	
Predicted Class	Dosed	383	0	100%
	Fresh	87	394	81.9%

TABLE IV: Classification Accuracy for LPMs 0, 2, and 4

Power Mode	Accuracy (%) (80 epochs)
LPM 0	84.7
LPM 2	93.5
LPM 4	89.9

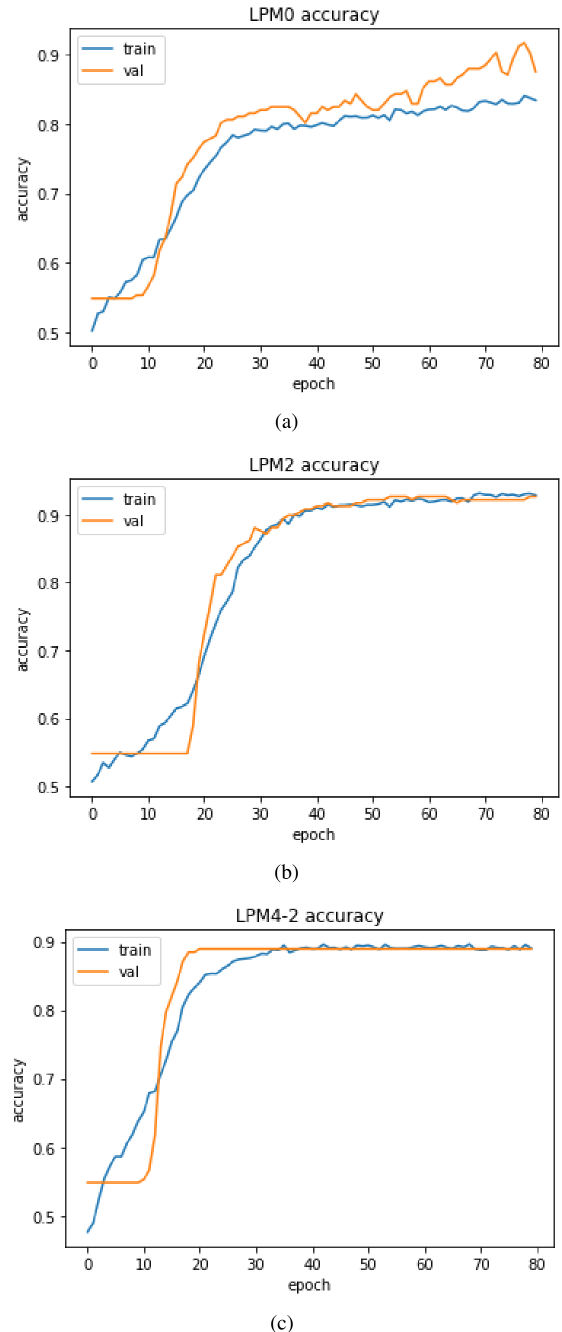

Fig. 5: Training (train) and validation (val) accuracy for up to 80 epochs for (a) LPM 0, (b) LPM 2, and (c) LPM 4.

B. Regression Model

The regression model was designed to predict the TID in krad(SiO_2) based on the noise, or standardized clock output, measured on the ACLK signal line. The CNN model was trained using back-propagation using a kernel size equal to the length of the time sample (at least 100 clock periods). The mean-squared error (MSE) was used as the loss function. The MSE measures how close a model's predictions are to the regression line. As the error is squared, the effect of negative values is removed, and the weights of significant errors are magnified. A lower MSE value equates to a better model. Fig. 6 shows the model reducing the training and validation MSE as the model learns in each epoch, meaning the model's predictions are becoming more accurate. The model performs best in the lowest power mode (LPM 4) and worst in the highest power mode (LPM 0).

The regression model's performance after being irradiated in LPM 4 is shown below in Fig. 7. The box plot statistics for the model's predictions are shown at each incremental dose point where data was collected. The dotted line represents the actual dose of the part. It can be seen that the predictions coarsely track the expected dose. Furthermore, information regarding how to best determine classifier bins can be gained using this plot. For example, the binary classifier presented here classifies a part with a dose below 25 krad(SiO_2) as fresh and above

25 krad(SiO_2) as dosed. However, it is seen that from 20 to 30 krad(SiO_2), the model's predictions stay relatively the same. Moreover, according to Fig. 1, the MCU performance remains relatively constant with dose until rapid degradation above 30 krad(SiO_2).

A simple solution to improve the accuracy of the binary classifier would be to shift the classification threshold from 25 to 30 krad(SiO_2), where a significant increase in the model's predictions occurs. Increasing the number of bins is another option that may lead to higher accuracy. The regression model is helpful for loosely tracking TID and understanding the device's response, which can help create a high-accuracy classifier.

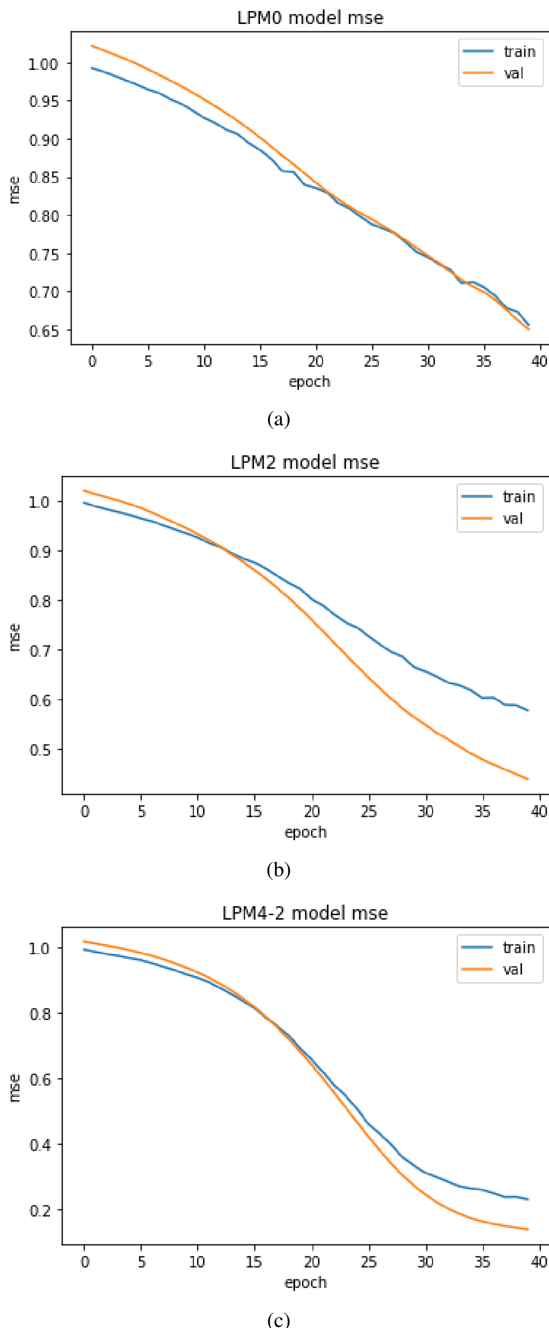

Fig. 6: Mean-squared error (MSE) training (train) and validation (val) data versus epoch for the TID regression models for DUTs biased in (a) LPM 0, (b) LPM 2, and (c) LPM 4.

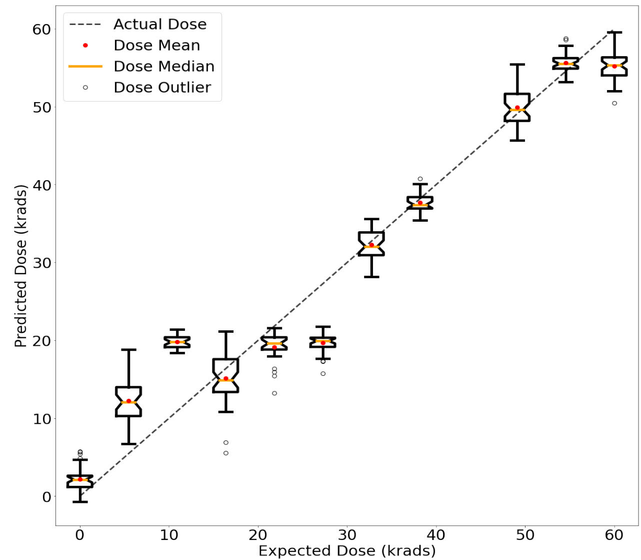

Fig. 7: Regression Model Predictions versus Expected Dose.

VI. Conclusions

This paper describes two methodologies for using machine learning (ML) to predict an SoC's total ionizing dose (TID). First, a binary classifier based on a convolutional neural network (CNN) was used to classify devices as either being new/unirradiated or dosed over 25 krad(Si)O2). Second, CNN-based regression was used to build predictive TID models by minimizing the mean-squared error (MSE).

Data were collected from X-ray exposures of TI MSP430FR6989 mixed-signal microcontroller units (MCU) under irradiation in various sleep states or low-power modes. The models were trained with the noise signatures obtained from the output of the processor clock signals. The regression model effectively predicts the TID value with an MSE as low as 0.14. The classification model results in accuracy up to 93.5% with positive predictive values (PPV) as high as 100%. Additionally, the models were sensitive to DUT bias under irradiation, performing worse when modules were active.

The regression and classification models demonstrate the ability to use ML to analyze TID. The ML model can also be easily trained on other data such as clock frequency, analog-to-digital (ADC) converter output, power consumption, or other electrical characteristics, and thus varying degrees of accuracy may be obtained in the future. Once the ML models are trained with prior test data, it is possible to deploy them on FPGA devices included on critical missions to perform real-time analysis of TID. A similar method may also be used to predict displacement damage. Real-time knowledge of system health concerning TID is a metric that can be utilized to diagnose and address issues while a mission is active.

References

[1] R. Netzer, K. Avery, W. Kemp, A. Vera, B. Zufelt, and D. Alexander, "Total ionizing dose effects on commercial electronics for cube sats in low earth orbits," in *2014 IEEE Radiation Effects Data Workshop (REDW)*, 2014, pp. 1–7.

[2] H. Quinn, W. H. Robinson, P. Rech, M. Aguirre, A. Barnard, M. Desogus, L. Entrena, M. Garcia-Valderas, S. M. Guertin, D. Kaeli, F. L. Kastensmidt, B. T. Kiddie, A. Sanchez-Clemente, M. S. Reorda, L. Sterpone, and M. Wirthlin, "Using benchmarks for radiation testing of microprocessors and fpgas," *IEEE Transactions on Nuclear Science*, vol. 62, no. 6, pp. 2547–2554, 2015.

[3] S. M. Guertin, R. Some, P. Nsengiyumva, E. H. Cannon, M. Cabanas-Holmen, and J. Ballast, "Radiation specification and testing of heterogenous microprocessor socs," in *2019 19th European Conference on Radiation and Its Effects on Components and Systems (RADECS)*, 2019, pp. 1–7.

[4] N. Rezzak, J.-J. Wang, M. Traas, A. Zerrouki, G. Bakker, F. Xue, A. Cai, F. Hawley, J. McCollum, and E. Hamdy, "Investigation of tid and dynamic burn-in-induced v_T shift on rtg4 flash-based fpga," *IEEE Transactions on Nuclear Science*, vol. 65, no. 1, pp. 64–70, 2018.

[5] W. Rice, M. Marquez, T. Jaswal, S. Caruso, and A. R. Gil, "Response of a 22fdx® radiation-hardened-by-design test chip to tid and see," in *2021 IEEE Radiation Effects Data Workshop (REDW)*, 2021, pp. 1–4.

[6] C. M. Szabo, A. Duncan, K. A. LaBel, M. Kay, P. Bruner, M. Krzesniak, and L. Dong, "Preliminary radiation testing of a state-of-the-art commercial 14nm cmos processor / system-on-a-chip," in *2015 IEEE Radiation Effects Data Workshop (REDW)*, 2015, pp. 1–8.

[7] B. Bhat, N. Upadhyaya, and R. Kulkarni, "Total radiation dose at geostationary orbit," *IEEE Transactions on Nuclear Science*, vol. 52, no. 2, pp. 530–534, 2005.

[8] S. Kumar, A. K. Srivastava, and B. Umapathi, "Development of floating gate mosfet for dosimeter," in *2016 IEEE Annual India Conference (INDICON)*, 2016, pp. 1–4.

[9] S. T. Vibbert, A. C. Watkins, J. V. D'Amico, M. W. McKinney, D. S. Vibbert, E. X. Zhang, D. R. Ball, T. D. Haeffner, M. L. Alles, J. S. Kauppila, and L. W. Massengill, "In situ measurement of tid-induced leakage using on-chip frequency modulation," *IEEE Transactions on Nuclear Science*, vol. 69, no. 3, pp. 367–373, 2022.

[10] B. Patel, M. Joplin, R. C. Boggs, D. R. Reising, M. W. McCurdy, L. W. Massengill, and T. D. Loveless, "Ionizing radiation effects spectroscopy for analysis of total-ionizing dose degradation in rf circuits," *IEEE Trans. Nucl. Sci.*, vol. 66, no. 1, pp. 61–68, Jan. 2019.

[11] T. D. Loveless, B. Patel, D. R. Reising, R. Roca, M. Allen, L. W. Massengill, and D. McMorrow, "Ionizing radiation effects spectroscopy for analysis of single-event transients," *IEEE Trans. Nucl. Sci.*, vol. 67, no. 1, pp. 99–107, Jan. 2020.

[12] T. D. Loveless, D. R. Reising, J. C. Cancelleri, L. W. Massengill, and D. McMorrow, "Analysis of single-event transients (sets) using machine learning (ml) and ionizing radiation effects spectroscopy (ires)," *IEEE Transactions on Nuclear Science*, vol. 68, no. 8, pp. 1600–1606, 2021.

[13] J. R. Srour and J. W. Palko, "Displacement damage effects in irradiated semiconductor devices," *IEEE Transactions on Nuclear Science*, vol. 60, no. 3, pp. 1740–1766, 2013.